Glioma–macrophage interaction through mathematical modeling of EGF-CSF-1 pathway in brain tumors

Soheila Zeinali [a] and **Meltem Elitas [a]**

[a]Sabanci Universtiy, Universite Cd., No: 27, Tuzla, Istanbul, Turkey

szeinali@sabanciuniv.edu and melitas@sabanciuniv.edu

Corresponding author: Meltem Elitas

Abstract

Glioblastoma multiform (GBM) is one of the most lethal forms of brain cancers. The biggest difficulties for diagnostics and treatment of GBM underlie in its dynamic and complex macro and microenvironment. Glioma cells, stromal cells and tumor-associated immune cells (microglia/macrophage-TAMs) become a complex tissue with physical and chemical communication network. TAMs are the predominant infiltrating immune cells in malignant GBMs and stimulate tumor invasion, angiogenesis, and metastasis. The epidermal growth factor (EGF) and colony stimulating factor 1 (CSF-1) paracrine signaling loop plays a key role in communication between glioma cells and TAMs. We developed a mathematical model to investigate macrophage-glioma cell interactions using CSF-1 and EGF paracrine-acting agents. Our model presents change of EGF and CSF-1 concentration both on the surfaces of cells and within a well-defined tumor microenvironment, in a domain, with respect to interaction time and distance between TAMs and glioma cells. Our simulation results confirm that from low-grade glioma to high-grade glioma, concentration of CSF-1 increases both on the surfaces of macrophages and within the domain. Therefore, reproduction and adsorption of CSF-1 correlates with the grade of malignancy in human gliomas, which is a good agreement with recent findings.

Keywords: Glioblastoma, signaling, simulation, invasiveness.

1. Introduction

Glioblastoma multiform (GBM) is one of the most lethal forms of brain cancer in humans. Survival of patients could be extended up to 15 months with chemotherapy, radiation and surgery[1-4] yet, multiple

challenge remains for better clinical outcomes[5, 6]. The biggest difficulties for diagnostic and treatment of GBM underlie in its complex macro and microenvironment. The macro environment of brain presents several complexities such as composing of several sensitive cell types to chemotherapeutic reagents; being surrounded by blood-brain barrier that limits delivery of drugs, and the skull that restricts growth of tumors. On the other hand, microenvironment of GBM is also highly complex, dynamic hierarchical cell society due to presence of diverse cell types with distinct phenotypes and different proliferative potentials. GBM cells co-evolve with stromal and tumor-associated immune cells (microglia/macrophage) and form complex physical and chemical cell-cell communication network. TAMs are abundant and the predominant infiltrating immune cells in malignant GBMs, which are present at World Health Organization (WHO) grade II-IV gliomas[7-10]. During tumor progression, macrophages can stimulate tumor invasion, angiogenesis, and metastasis[11]. Although the role of infiltrated macrophages in tumor progression has been recognized, still the precise nature of the interaction mechanisms between tumor cells and macrophages has not been elucidated[12]. Mills et al. extended an in vivo model for the function of TAMs and suggested two states of TAMs as activated (M1) and alternatively activated (M2) macrophages. M1 and M2 TAMs differ in activating signals, expression of receptors, cytokine production and biological behavior. This suggestion describes that TAMs with M1 polarization are foes and TAMs with M2 polarization are friends for tumors[7, 13]. Tumor-derived molecules, such as colony-stimulating factor 1 (CSF-1), can polarize glioma-infiltrating macrophages towards M2 polarization and result in production of anti-inflammatory molecules[14-16] and epidermal growth factor (EGF), which acts in return on EGF receptor (EGFR) on the carcinoma cells to promote invasion[17]. EGF-CSF-1 signaling affects the ratio of cell types in aggregates and enables glioma cells to infiltrate into the brain parenchyma[5]. Since GBMs are highly complex with unpredictable patterns, several mathematical models have been used to reveal its complexity and predict its progress[18, 19]. Particularly, compared to other scientific boards, neuro-oncology still requires more effort to propose predictive tools that could accurately simulate the behavior of malignant gliomas[20, 21]. Martirosyan and his coworkers summarized the mathematical models that describe different aspects of GBM growth and evaluation such as spheroid models, metabolic and vascular models, morphological models, and treatment models[20].

Among them, spheroid models represent a powerful theoretical framework to study initial growth of GBM when proliferation and diffusion of glioblastoma cells are the major players in the tumor initiation. These types of models composed of reaction-diffusion models, simple discrete models and continuum models. Stein et al. used bright field image sequences to estimate number of cells in the tumor spheroids and described a continuum mathematical model to quantitatively interpret the data. After fitting quantitative and experimental data, they observed that glioma cells with EGF receptor show less cell-cell adhesion and invade in a more biased manner and greater rate[22]. Banerjee et al. developed a mathematical model considering the interactive dynamics of glioma cells, macrophages, cytotoxic T-lymphocytes and T11 Target structure (T11TS), which is a membrane glycoprotein and affects the functional state of immune cells. Their model concluded that T11T structure might be used as a drug target for effective treatment of brain tumors[6]. Aubert and Bandoual proposed a two dimensional model that quantified the strength of cell-cell adhesion using a probability threshold. The agreement of mathematical modeling with experimental results approved that cell-cell adhesion is extremely important for the growth and behavior of glioma cells[23, 24]. Considering biased diffusion in glioblastoma, Fort and Sole's improved standard reaction-diffusion-advection model pointed that glioma cells move in a bias towards the invasion front instead of moving equally in all directions. It provides a great agreement with experiments[25].

The vascular and metabolic models are related to invasiveness and aggressiveness of the tumor that requires more nutrient supply consequently; these models oftentimes predict the onset of angiogenesis and creation of vasculature[20]. In this concept, some models analysed collective cell migration, tumor cell spatial distribution, morphology and viability using conservation laws[26-28]. Some models were compartmentalized via dividing tumor cell populations into normal, hypoxic, and necrotic cell groups to cover all dynamics of tumor microenvironment[19, 29-31]. Some models investigated the phenotypic switch that occurs from proliferative state to invasive state in glioma cells as function of hypoxia[32]. The morphological models uses discrete models and reaction-diffusion models to investigate the microscopic and macroscopic morphological changes, glioma growth, invasion based on cell-cell and cell-extracellular matrix adhesion, hypoxia, chemotaxis, homotype attractions, substrate gradients (glucose, oxygen) and other microenvironmental parameters[33-36]. In the treatment models the ultimate goal is providing solutions for

better treatment outcome, prolonging and improving patient life. As mentioned, treatment of glioblastoma is not very efficient compared to other cancer types and better strategies are urgently needed. The modeling strategies target better treatment regimen using radiotherapy, chemotherapy, patient MRI data and resection in conjunction with two-, three- and four-dimensional computer modeling systems[37]. Thus, chemotherapy and radiotherapy is able to simulated with different drugs[38] and dose schedules, partial resection of tumor and filling the ablated volume with different chemicals such as cerebrospinal fluid, chemoattractants[39].

Despite efforts to understand the dynamics of glioma cells and macrophage interactions, little data is available to suggest the partnership between glioma cells and M2 type TAMs. However, most of the findings are based on human end-stage tumor samples obtained from surgical secretions. In order to reveal the nature of interaction between glioma cells and macrophages, efforts may focus on studying the nature of interaction between glioma cells and macrophages arises at tumor onset[8]. Based on the need for better understanding of the macrophage-tumor cell interactions in tumor microenvironment, mathematical models, which reveal and simulate the nature of these interactions, are of high challenge and consideration. In this work, we present a computational model for further investigation of macrophage-glioma cell interactions focusing on concentration change of paracrine-acting agents (CSF-1 and EGF) in a defined microenvironment (domain) and on the cellular surfaces.

2. Model

Recent clinical experiments reported that TAMs facilitate invasiveness of GBM through EGF-CSF-1 paracrine signaling loop[17]. Macrophages secrete EGF and respond to CSF-1; similarly glioma tumor cells express CSF-1 and respond to EGF via chemotaxis, **Figure 1**. This cooperation enables glioma cells to coordinate their aggregation and migration via macrophage-facilitated dissemination from primary tumor to surrounding healthy brain tissue [5, 16, 17]. To reveal the interaction mechanism between glioma cells and macrophages, we developed a computational model and simulate the EGF and CSF-1 paracrine loop both on the cell surfaces and in a domain consist of macrophages and glioma tumor cells. **Figure 1a** illustrates EGF and CSF-1 interaction loop at single cell level while the schematic in **Figure 1b** demonstrates EGF and CSF-1 interaction in a domain at population level.
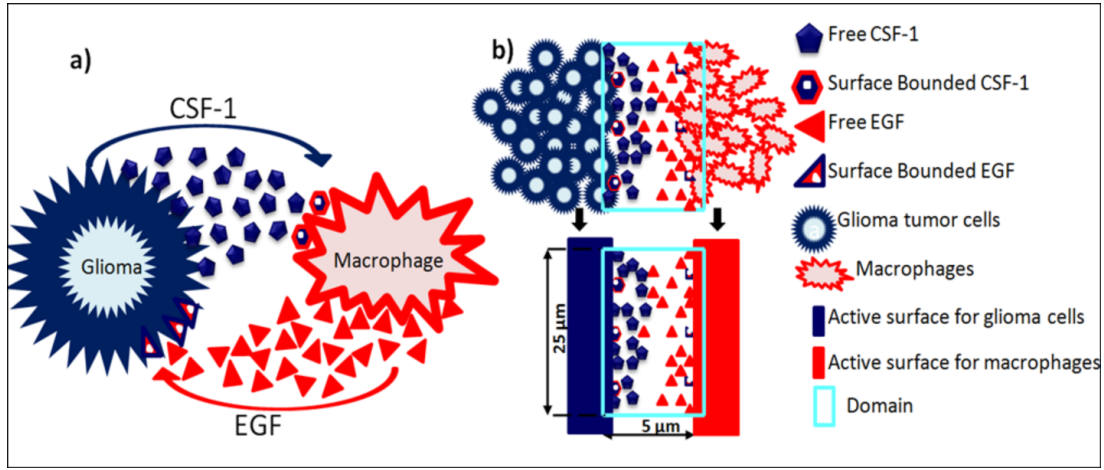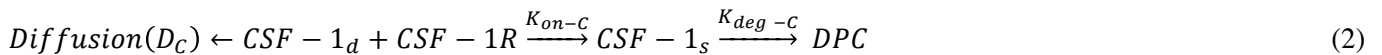
Figure 1: Schematics for the EGF-CSF1 signaling loop. a) Macrophage and glioma cell interact through EGF-CSF-1 signaling loop. Glioma cells secrete CSF-1 and it binds to macrophages and makes them express EGF, which acts on CSF-1 secretion of glioma tumor cells. b) Schematic of 2D simulation domain to use reaction-diffusion models. Active surface for glioma cells represents the community of glioma cells and active surface for macrophages describes the community of macrophages present in the modeling domain. As a case study, it is assumed that these two communities have size of 25 μm as length of active surfaces and are in the distance of 5 μm from each other.

In our modeling, we numerically solve the equations that govern the movement and binding of CSF-1 and EGF. Fick's second law explains diffusive transport, where D is the diffusion coefficient. C is the concentration of species, Δ is Laplacian and t is time.

$$\partial C/\partial t = D\Delta C \tag{1}$$

Incorporating reaction-diffusion modeling, the nature of interaction in the paracrine signaling loop is described as follows[40]:

$$Diffusion(D_C) \leftarrow CSF-1_d + CSF-1R \xrightarrow{K_{on-C}} CSF-1_s \xrightarrow{K_{deg-C}} DPC \tag{2}$$

$$Diffusion(D_E) \leftarrow EGF_d + EGFR \xrightarrow{K_{on-E}} EGF_s \xrightarrow{K_{deg-E}} DPE \tag{3}$$

CSF-1R represents the concentration of receptors on macrophage cell surface for binding of CSF-1 secreted by glioma cells and EGFR represents the concentration of receptors located on glioma cell surface for binding of EGF secreted by macrophages. K_{on-C} and K_{on-E} incorporate the rate constants for CSF-1R and EGFR binding, respectively. Moreover, CSF-1$_s$ and EGF$_s$ are surface species and represent the concentration of bound CSF-1 on the macrophage and bound EGF on the glioma cell surfaces. K_{deg-C} and K_{deg-E} are the rate constants for degradation of CSF-1$_s$ and EGF$_s$. DPC and DPE are the degradation of products. The CSF-1$_d$ and EGF$_d$ are bulk species in the domain and introduced at the rate of ϑ_C and ϑ_E at specific locations and have effective diffusion coefficient of D_C and D_E, respectively. In our calculations, including surface reaction and bulk diffusion expressions (2) and (3) are described with the following equations [40]:

$$\partial CSF\text{-}1_d/\partial t = D_C.\Delta CSF\text{-}1_d + \vartheta_C \tag{4}$$

$$\partial CSF\text{-}1_s/\partial t = K_{on-C}.CSF\text{-}1_d.(1 - CSF\text{-}1_s) - K_{deg-C}.CSF\text{-}1_s \tag{5}$$

$$\partial EGF_d/\partial t = D_E.\Delta EGF_d + \vartheta_E \tag{6}$$

$$\partial EGF_S/\partial t = K_{on-E}.EGF_d.(1 - EGF_s) - K_{deg-E}.EGF_s \tag{7}$$

Equations (4) and (6) are surface-reaction expressions and include the concentrations of free species (CSF-1$_d$ and EGF$_d$) and should be solved in combination with the mass balance of species in the domain. The coupling between bulk and surface expressions is obtained as boundary condition in the bulk's mass expressions (equations (4) and (6)), which sets the flux of CSF-1$_d$ and EGF$_d$ at the active surfaces.

Our mathematical model is based on the following assumptions:

- The physical and chemical properties of domain and surface CSF-1 and EGF reagents are uniform and continuous.

- The mass balance of the domain has been coupled to the mass balances of CSF-1 and EGF present on the active surfaces.

- The initial condition concentrations of CSF-1 and EGF are zero.

For the domain species, the boundary conditions at active surfaces couple the rate of the reactions at the surfaces with the concentration of free species in the domain:

$$(-D_C.\nabla CSF\text{-}1_d) = -K_{on\text{-}C}. CSF\text{-}1_d.(1 - CSF\text{-}1_s) \tag{8}$$

$$(-D_E.\nabla VEGF_d) = -K_{on\text{-}E}. EGF_d.(1 - EGF_s) \tag{9}$$

In order to couple the reaction-diffusion expressions of CSF-1 and EGF, we have assumed that $K_{on\text{-}E}$ varies based on the concentration of macrophages and glioma cells in the domain and a linear correlation occurs between ϑ_C, ϑ_E, $K_{on\text{-}C}$ and $K_{on\text{-}E}$ as follows,

$$\vartheta_C/\vartheta_E = K_{on\text{-}C} / K_{on\text{-}E} \tag{10}$$

Therefore, the value of $K_{on\text{-}E}$ for each glioma grade could be determined from equation (10). Definitions, default values and their references are provided in **Table 1**.

The mathematical modeling deals with a diffusion occurring in a 2D domain, which is coupled, to a surface reaction phenomenon occur on a part of the domain's boundary. The phenomenon in the domain refers to introduction of $CSF\text{-}1_d$ from the glioma and EGF_d from the macrophages as sources and the surface phenomenon describes the binding of species from the domain to the active surfaces that reactions take place.

Parameter	Symbol	Value	Units	References
Diffusion of $CSF1_f$	D_C	1.6×10^{-10}	m^2/s	41
Diffusion of EGF_f	D_E	1.6×10^{-10}	m^2/s	41
Degradation of $CSF1_b$	$K_{deg\text{-}C}$	1.9×10^{-4}	1/s	42
Degradation of EGF_b	$K_{deg\text{-}E}$	1.9×10^{-4}	1/s	42
Secretion rate of $CSF1_f$	ϑ_C / N_g	1.7×10^{-23}	$mol/m^3.s$	43
Secretion rate of EGF_f	ϑ_E / N_g	1.7×10^{-23}	$mol/m^3.s$	44
Binding rate of $CSF1_f$	$K_{on\text{-}C}$	7.7×10^4	$mol/m^3.s$	45

***Table 1:** Table of parameters, their values and references used in simulation.*

Equations (4) and (6) are modeled using Transport of Diluted Species interface and equations (5 and 7) are described with General Form Boundary PDE interface in COMSOL Multiphysics 5. The equations of two interfaces are coupled considering expressions (8) and (9) as boundary conditions.

The concentration of species in the domain and on the surfaces of the cells has been affected from the interaction of macrophages and glioma cells that are present in the domain. In this study, WHO grade I-IV gliomas are considered based on the concentration of glioma and macrophages. **Table 2** describes number of macrophages and glioma cells at each grade of glioma brain cancer[46]. We calculated the value of K_{on-E} using equation (12) and using the number of macrophages and glioma cells in **Table 2**[47].

WHO grades	Macrophage (N_m)	Glioma (N_g)	K_{on-E}
I	2×10^7	16×10^6	6.1×10^4
II	1×10^7	56×10^6	4.3×10^5
III	2×10^6	16×10^7	2.5×10^6
IV	1×10^6	26×10^7	2×10^7

Table 2: *The number of cells and the values of K_{on-E} used in simulations were used from Dr. Lu and his co-workers study[47].*

3. Results

In this work, we have developed a continuum mathematical model that simulates the concentrations of EGF and CSF-1 paracrine reagents for the surface-bounded species on the active surfaces of macrophages, $CSF\text{-}1_s$ (mol/m^2) and on the active surfaces of glioma tumor cells, EGF_s (mol/m^2), the secreted $CSF\text{-}1_d$ (mol/m^3) and EGF_d (mol/m^3) as bulk concentrations (free reagents) in the domain. The simulations were performed for 24 hours. **Figure 2** shows the schematic view and the change of $CSF\text{-}1_d$ after 24 hours of interaction between macrophages and glioma tumor cells in the domain for all WHO grades of gliomas (I (a), II (b), III (c) and IV (d)). According to modeling results, all color tables of **Figure 2** are assigned to have 1.76×10^{-26} as minimum (blue) and 3.45×10^{-16} (red) as maximum reference values for $CSF\text{-}1_d$.

Likewise, **Figure 3** shows the concentration gradient of EGF_d after 24 hours interaction among macrophages and glioma tumor cells in the domain. The reference minimum value of EGF_d is 4.25×10^{-30}

(blue) and the reference maximum value is 2.67×10^{-17} (red) for the color table. The schematic images represent that the ratio for number of glioma cells to number of macrophages. Grade I glioma is close to 1, this ratio increases from grade I to grade IV, and reaches 260 at grade IV glioma.
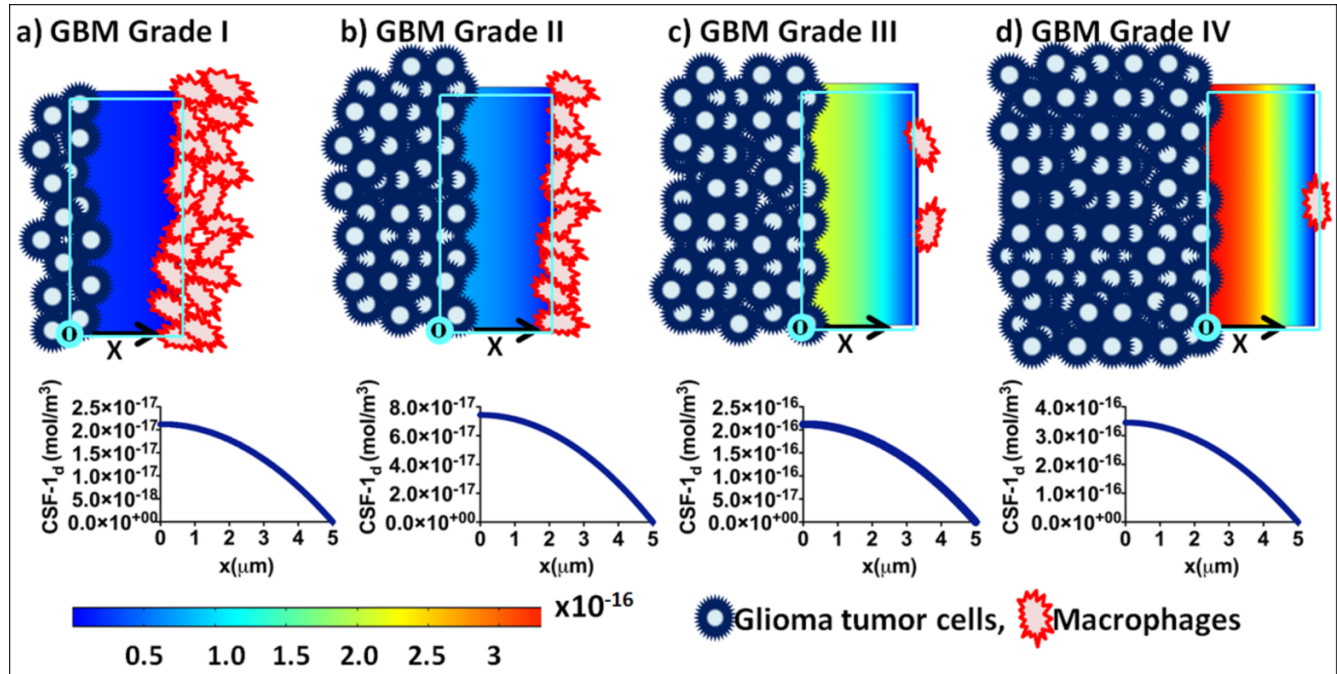

Figure 2: Concentrations of CSF-1_d within the domain after 24 hours of macrophage-glioma cell interaction. *The schematic images symbolize the WHO grades of the glioma including 2D-color table, which represents the concentration gradient of CSF-1d, and one-dimensional plot presents the change in the concentration of CSF-1_d in x-direction of the domain.* ***a)*** *The grade I glioma with $2x10^7$ macrophages and $16x10^6$ gliomas,* ***b)*** *the grade II glioma with $1x10^7$ macrophages and $56x10^6$ glioma cells,* ***c)*** *the grade III glioma with $2x10^6$ macrophages and $16x10^7$ glioma cells, and* ***d)*** *the grade IV glioma with $1x10^6$ macrophages and $26x10^7$ glioma cells. For all grades of glioma, the initial concentration value of CSF-1_d was set to zero. The simulation time was 24 hours. All color tables are assigned to have minimum (blue) and maximum (red) reference values of $1.76x10^{-26}$ and $3.45x10^{-16}$, respectively. Glioma cells and macrophages are located on their specific active surfaces and the number of cells in each image illustrates, in a symbolic way, the difference between the number of glioma cells and macrophages. The x-axis stands for the distance between macrophages and glioma cells; the origin is located at the active surface of glioma cells.*
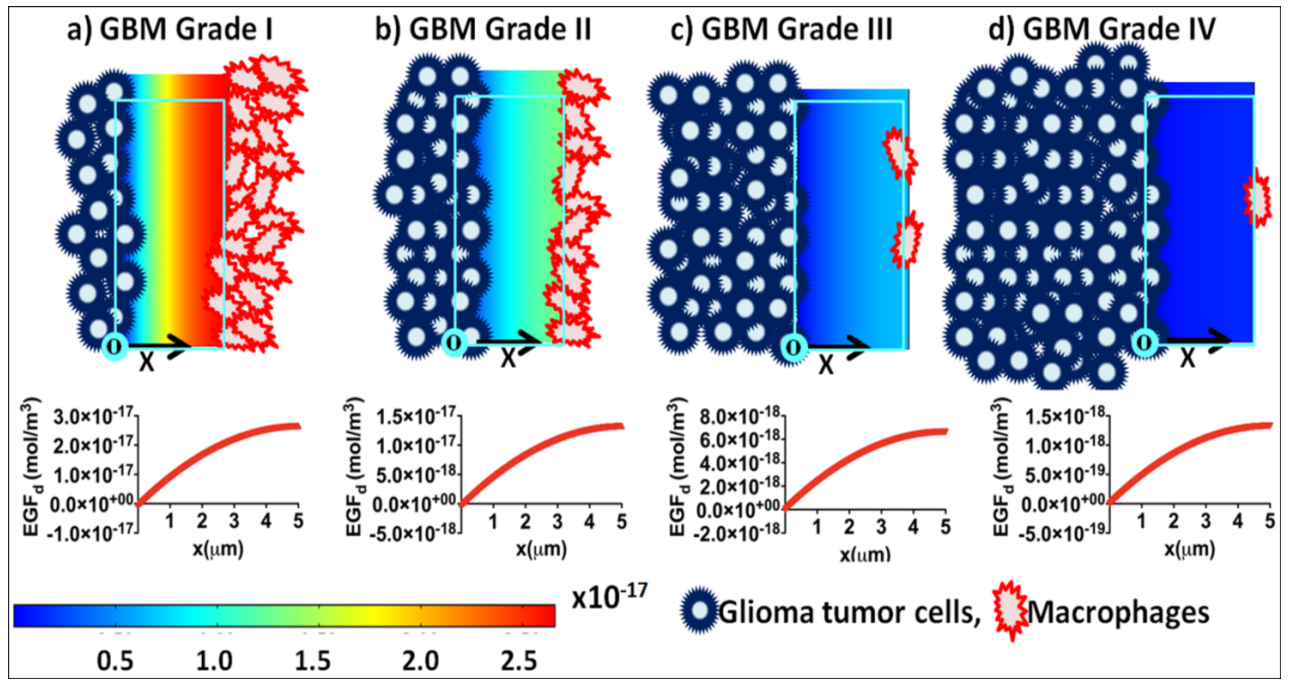
Figure 3: Concentrations of EGF$_d$ within the domain after 24 hours of macrophage-glioma cell interaction. The schematic images symbolize the WHO grades of the glioma including 2D-color table, which represents the concentration gradient of EGF$_d$, and one-dimensional plot presents the change in the concentration of EGF$_d$ in x-direction of the domain. a) The grade I glioma with $2x10^7$ macrophages and $16x10^6$ glioma cells, b) the grade II glioma with $1x10^7$ macrophages and $56x10^6$ glioma cells, c) the grade III glioma with $2x10^6$ macrophages and $16x10^7$ glioma cells, and d) the grade IV glioma with $1x10^6$ macrophages and $26x10^7$ glioma cells. For all grades of glioma, the initial concentration value of EGF$_d$ was set to zero. The simulation time was 24 hours. All color tables are assigned to have minimum (blue) and maximum (red) reference values of $4.25x10^{-30}$ and $2.67x10^{-17}$, respectively. Glioma cells and macrophages are located on their specific active surfaces and the number of cells in each image illustrates, in a symbolic way, the difference between the number of glioma cells and macrophages. The x-axis stands for the distance between macrophages and glioma cells; the origin is located at the active surface of glioma cells.

One-dimensional plots in **Figure 2** and **Figure 3** illustrate the change in the concentration of CSF-1$_d$ and EGF$_d$ in x-direction of the domain for each stage. The x-axis represents the average displacement between the population of glioma cells and macrophages; it starts from the active surface of glioma cells (x = 0μm) and ends at the active surface of macrophages (x = 5μm). Consequently, the concentration of CSF-1$_d$ decreases through the x-direction of the domain and reaches the approximate value of zero at x=5μm.
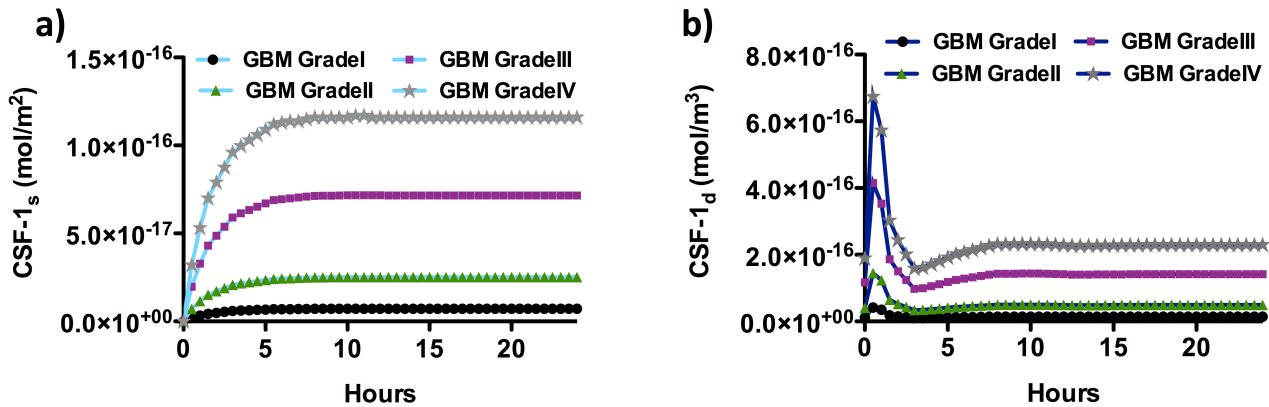

Figure 4: Time-dependent concentration changes for CSF-1$_s$ and CSF-1$_d$ for low-grade to high-grade gliomas. a) Concentration of CSF-1$_s$ with respect to time from low-grade glioma to high-grade glioma. b) Concentration of CSF-1$_d$ with respect to time from low-grade glioma to high-grade glioma. The initial concentration values of CSF-1$_s$ and CSF-1$_d$ were zero. The simulations were performed for 24 hours. The grade I glioma has $2x10^7$ macrophages and $16x10^6$ glioma cells, the grade II glioma has $1x10^7$ macrophages and $56x10^6$ glioma cells, the grade III glioma has $2x10^6$ macrophages and $16x10^7$ glioma cells, and the grade IV glioma has $1x10^6$ macrophages and $26x10^7$ glioma cells.
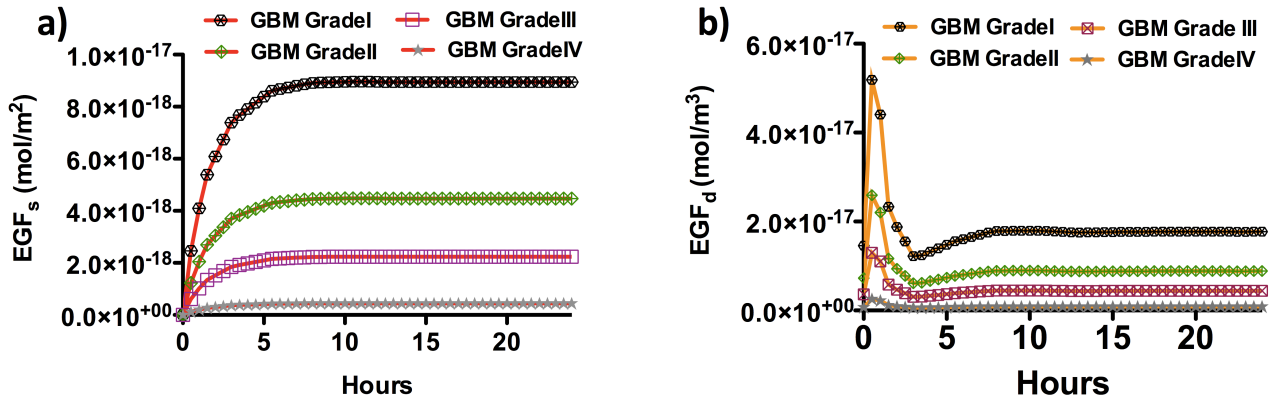
Figure 5: Time-dependent concentration changes for EGF_s and EGF_d for low-grade to high-grade gliomas. a) Concentration of EGF_s with respect to time from low-grade glioma to high-grade glioma. b) Concentration of EGF_d with respect to time from low-grade glioma to high-grade glioma. The initial concentration values of EGF_s and EGF_d were zero. The simulations were performed for 24 hours. The grade I glioma has $2x10^7$ macrophages and $16x10^6$ glioma cells, the grade II glioma has $1x10^7$ macrophages and $56x10^6$ glioma cells, the grade III glioma has $2x10^6$ macrophages and $16x10^7$ glioma cells, and the grade IV glioma has $1x10^6$ macrophages and $26x10^7$ glioma cells.

When the concentrations of adsorbed species on the cellular surface increase with time, the concentrations of domain species ($CSF-1_d$ and EGF_d) decrease due to adsorption by active surfaces and coupling of reaction and diffusion phenomena at all glioma grades. For the grade I glioma, the number of macrophages was 1.25 times higher than the number of glioma cells in the domain. At grade II gliomas, macrophages are 0.17 times of glioma cells in the domain and the concentration of $CSF-1_s$ and $CSF-1_d$ was approximately 5.5 times of the concentration of EGF_s and EGF_d. For grade III and IV gliomas the ratio of macrophages to glioma cells are 0.01 and 0.003 and the ratio of CSF-1 species to EGF species are approximately 32 and 260, respectively. From grade I to grade IV gliomas, the ratio of macrophages to glioma cells approximately uniformly decreased, but based on the observations from the modeling this approximate uniformity could not be generalized to the ratio of domain species to surface species at each grade of glioma.

12

Figure 4 shows that for both species of CSF-1, grade I glioma has minimum concentration and towards high-grade glioma, which means increasing in the ratio of glioma cells to macrophages, CSF-1 bulk and surface species experience higher concentrations. Despite the CSF-1 species, **Figure 5** illustrates that EGF species have the minimum concentrations for grade IV gliomas where the ratio of macrophages to glioma cells is the minimum.

4. Conclusions

We have presented a simple 2D co-culture model that investigates CSF-1 and EGF interaction *in vitro* from grades I to IV human glioma disease. Our model represents the difference in the surface-bounded (CSF-1$_s$-EGF$_s$) and bulk expressed (CSF-1$_d$-EGF$_d$) paracrine-signaling reagents of CSF-1 and EGF both at spatial and temporal resolution. Although most of the current models focus on measuring the total concentration of signalling molecules in a defined domain, our model and prediction of the surface-bounded concentration of signaling reagents provide a great potential to improve our understanding for mechanism of interaction between glioma cells and tumor-associated immune cells in the concept of tumor invasiveness and grade of the disease. The importance of bulk and surface-bounded cytokine classification, particularly in the concept of CSF-1 expression in glioblastoma multiform, was reported in Graf's experimental paper in 1999[50]. Their conclusion was membrane-bound cytokines were more potent than its soluble counterparts.

Moreover, in our mathematical modeling, we observed that increasing the WHO grades of glioblastoma increases the concentration of CSF-1 both in the domain and on the surface of macrophages. However, the increase in the concentration of CSF-1 and decrease in the concentration of EGF do not obey the uniform change in the number of macrophages and glioma cells. In glioma microenvironment, macrophages depend upon CSF-1 for differentiation, migration and survival. Pyonteck *et al.*, found that CSF-1R inhibition blocks glioma unexpected growth, progression and invasion [48]. Therefore, CSF-1 is one of the main factors for macrophage and glioma survival in the glioblastoma multiform and its reproduction and adsorption needs to be increased from low to high-grade gliomas. Our mathematical

modeling approves the high reproduction of CSF-1 at high-grade gliomas as repoteted by Coniglio and his colleagues. They observed that CSF-1 levels were elevated in higher grade gliomas and approved that glioblastoma invasion completely depended on CSF-1R signaling [5]. Bender *et al.*, proposed that in a genetic screen for oncogenes driving astrocytomas, CSF-1 was regulated in nearly 70% of spontaneous astrocytomas[49]. In our mathematical model, increasing grade number of the disease results in elevating not only the bulk species, but also surface species of CSF-1. Glioma cells express more CSF-1 in the bulk and macrophages being affected from this high supply, adsorb more CSF-1 on their surfaces until the time to reach the steady state.

As our next goal, we are planning to incorporate the cellular information such as division time of cells in our model to correlate whether the levels of CSF-1 and EGF impact cellular behaviour and tumor growth such as invasiveness. It will potentially provide more insights for building disease prediction models.

Last but not least, our model simply allows introducing different types of cytokines (more signalling pathways) and cell types (glioma stem cells, astrocytes, and microglia) of glioma microenvironment while providing possibilities of upgrading from 2D to 3D microenvironment, where complexity, dynamic cellular distribution of different cell types and heterogeneity of glioma microenvironment will be more realistically mimicked and the obtained results will be extensively contributed to the development of personalized treatment and drug test models for human brain tumors.

References

1.   H. O. David N. Louis, Otmar D. Wiestler, Webster K. Cavenee, Peter C. Burger, Anne Jouvet, Bernd W. Scheithauer and Paul Kleihues, *Acta Neuropathol.*, 2007, **114**(97–109.

2.   M. Preusser, S. de Ribaupierre, A. Wöhrer, S. C. Erridge, M. Hegi, M. Weller and R. Stupp, *Annals of Neurology*, 2011, **70**, 9-21.

3.   R. Stupp, W. P. Mason, M. J. van den Bent, M. Weller, B. Fisher, M. J. B. Taphoorn, K. Belanger, A. A. Brandes, C. Marosi, U. Bogdahn, J. Curschmann, R. C. Janzer, S. K. Ludwin, T. Gorlia, A. Allgeier, D. Lacombe, J. G. Cairncross, E. Eisenhauer and R. O. Mirimanoff, *New England Journal of Medicine*, 2005, **352**, 987-996.

4.   M. B. T. Demuth *J Neurooncol.* , 2004, **70**, 217-228.

5.   S. J. Coniglio and J. E. Segall, *Matrix Biology*, 2013, **32**, 372-380.

6.   S. K. Sandip Banerjee , Swapna Chaudhuri, *PLoS One*, 2015, **10**, e0123611.

7.   R. Noy and Jeffrey W. Pollard, *Immunity*, **41**, 49-61.

8.   C. R. S. Benjamin C. Kennedy, David E. Anderson, Lisa Anderson, Peter Canoll, Jeffrey N. Bruce, and Richard C. E. Anderson, *Journal of Oncology*, **2013**, 11.

9.   L. M. AM Kostianovsky, RC Anderson, JN Bruce, DE Anderson., *J Immunol.* , 2008, **181**, 5425-5432.

10.   J. S. Rao, *Nat Rev Cancer*, 2003, **3**, 489-501.

11.   J. S. Jeon, S. Bersini, M. Gilardi, G. Dubini, J. L. Charest, M. Moretti and R. D. Kamm, *Proceedings of the National Academy of Sciences*, 2015, **112**, 214-219.

12.   M. Korbelik and M. R. Hamblin, *Photochemical & Photobiological Sciences*, 2015, **14**, 1403-1409.

13.   C. Mills, *Crit Rev Immunol.* , 2012, **32**, 463-488.

14.   W. Li and M. B. Graeber, *Neuro-Oncology*, 2012, **14**, 958-978.

15.   T. G. Douglass, L. Driggers, J. G. Zhang, N. Hoa, C. Delgado, C. C. Williams, Q. Dan, R. Sanchez, E. W. B. Jeffes, H. T. Wepsic, M. P. Myers, K. Koths and M. R. Jadus, *International Immunopharmacology*, 2008, **8**, 1354-1376.

16.   J. B. Wyckoff, Y. Wang, E. Y. Lin, J.-f. Li, S. Goswami, E. R. Stanley, J. E. Segall, J. W. Pollard and J. Condeelis, *Cancer Research*, 2007, **67**, 2649-2656.

17.   S. Goswami, E. Sahai, J. B. Wyckoff, M. Cammer, D. Cox, F. J. Pixley, E. R. Stanley, J. E. Segall and J. S. Condeelis, *Cancer Research*, 2005, **65**, 5278-5283.

18.   D. K. Mitsutoshi Nakada , Takuya Watanabe , Yutaka Hayashi , Lei Teng , Ilya V. Pyko and Jun-Ichiro Hamada *Cancers*, 2011, **3**, 3242-3278.

19.   K. R. Swanson, R. C. Rockne, J. Claridge, M. A. Chaplain, E. C. Alvord and A. R. A. Anderson, *Cancer Research*, 2011, **71**, 7366-7375.

20.   E. R. NL Martirosyan, WL Ramey, EJ Kostelich, Y Kuang Y, MC Preul., *Math Biosci Eng.* , 2015, **12**, 879-905.

21.   H. HATZIKIROU, A. DEUTSCH, C. SCHALLER, M. SIMON and K. SWANSON, *Mathematical Models and Methods in Applied Sciences*, 2005, **15**, 1779-1794.

22.   T. D. Andrew M. Stein, David Mobley, Michael Berens, and Leonard M. Sander, *Biophys J.* , 2007, **92**, 356–365

23.   M. B. M Aubert , S Féreol, C Christov, B Grammaticos *Phys Biol.* , 2006, **13**, 93-100.

24.   C. D. M Badoual , M Aubert, B Grammaticos *Phys Biol.* , 2010, **7**, 046013.

25.   F. Joaquim and V. S. Ricard, *New Journal of Physics*, 2013, **15**, 055001.

26.   S. C. Ferreira, M. L. Martins and M. J. Vilela, *Physical Review E*, 2002, **65**, 021907.

27.   H. B. Frieboes, J. S. Lowengrub, S. Wise, X. Zheng, P. Macklin, E. L. Bearer and V. Cristini, *NeuroImage*, 2007, **37, Supplement 1**, S59-S70.

28.   H. B. Frieboes, X. Zheng, C.-H. Sun, B. Tromberg, R. Gatenby and V. Cristini, *Cancer Research*, 2006, **66**, 1597-1604.

29.   A. Martínez-González, G. Calvo, L. Pérez Romasanta and V. Pérez-García, *Bull Math Biol*, 2012, **74**, 2875-2896.

30.   P. K. Maria Papadogiorgaki, Xenofon Kotsiakis and Michalis E Zervakis *Theoretical Biology and Medical Modelling* 2013, **10**, 47.

31.   G. C. Mindy D. Szeto, Jennifer Hadley, Russ Rockne, Mark Muzi, Ellsworth C. Alvord, Jr, Kenneth A. Krohn, Alexander M. Spence, and Kristin R. Swanson, *Cancer Res.*, 2009, **69**, 4502–4509. .

32. H. Hatzikirou, D. Basanta, M. Simon, K. Schaller and A. Deutsch, *Mathematical Medicine and Biology*, 2012, **29**, 49-65.

33. T. D. LM Sander, *Phys Rev E Stat Nonlin Soft Matter Phys.* , 2002, **66**, 051901.

34. S. Turner and J. A. Sherratt, *Journal of Theoretical Biology*, 2002, **216**, 85-100.

35. S. Gao and X. Wei, *Applicable Analysis*, 2012, **92**, 1379-1392.

36. E. L. Bearer, J. S. Lowengrub, H. B. Frieboes, Y.-L. Chuang, F. Jin, S. M. Wise, M. Ferrari, D. B. Agus and V. Cristini, *Cancer Research*, 2009, **69**, 4493-4501.

37. J. Tian, A. Friedman, J. Wang and E. A. Chiocca, *J Neurooncol*, 2009, **91**, 287-293.

38. G. S. Stamatakos, V. P. Antipas, N. K. Uzunoglu and R. G. Dale, *The British Journal of Radiology*, 2006, **79**, 389-400.

39. S. E. Eikenberry, T. Sankar, M. C. Preul, E. J. Kostelich, C. J. Thalhauser and Y. Kuang, *Cell Proliferation*, 2009, **42**, 511-528.

40. M. Kerszberg and L. Wolpert, *Journal of Theoretical Biology*, 1998, **191**, 103-114.

41. R. G. Thorne, S. Hrabětová and C. Nicholson, *Journal of Neurophysiology*, 2004, **92**, 3471-3481.

42. H. J. Ross, L. A. Moy, R. Kaplan and R. A. Figlin, *Cancer*, 1991, **68**, 441-443.

43. K. S. Taizo Nitta, Mark Allegretta, Stefan Brocke, Mae Lim, Dennis J. Mitchell, Lawrence Steinman, *Brain Research*, 1992, **1**, 19-25.

44. S. H. K Mishima , A Asai, K Yamaoka, Y Nagashima, N Taniguchi, C Kitanaka, T Kirino, Y Kuchino *Acta Neuropathol.* , 1998, **96**, 322-328.

45. X. Ma, Wei Y. Lin, Y. Chen, S. Stawicki, K. Mukhyala, Y. Wu, F. Martin, J. F. Bazan and Melissa A. Starovasnik, *Structure*, 2012, **20**, 676-687.

46. Y. Wu, Y. Lu, W. Chen, J. Fu and R. Fan, *PLoS Comput Biol*, 2012, **8**, e1002355.

47. Y. L. Yu Wu, Weiqiang Chen, Jianping Fu,Rong Fan, *PLoS Comput Biol*, 2012, **8**, e1002355.

48. S. M. Pyonteck, L. Akkari, A. J. Schuhmacher, R. L. Bowman, L. Sevenich, D. F. Quail, O. C. Olson, M. L. Quick, J. T. Huse, V. Teijeiro, M. Setty, C. S. Leslie, Y. Oei, A. Pedraza, J. Zhang, C. W. Brennan, J. C. Sutton, E. C. Holland, D. Daniel and J. A. Joyce, *Nat Med*, 2013, **19**, 1264-1272.

49. A. M. Bender, L. S. Collier, F. J. Rodriguez, C. Tieu, J. D. Larson, C. Halder, E. Mahlum, T. M. Kollmeyer, K. Akagi, G. Sarkar, D. A. Largaespada and R. B. Jenkins, *Cancer Research*, 2010, **70**, 3557-3565.

50. M. R. Graf, M. R. Jadus, J. C. Hiserodt, H. T. Wepsic and G. A. Granger, *The journal of Immunology*, 1999, **163**,5544-5551.

Table and figure legends:

Figure 1: Schematics for the EGF-CSF1 signaling loop. a) Macrophage and glioma cell interact through EGF-CSF1 signaling loop. Glioma cells secrete CSF1 and it binds to macrophages and makes them express EGF, which acts on CSF1 secretion of glioma tumor cells. b) Schematic of 2D simulation domain to use reaction-diffusion models. Active surface for glioma cells represents the community of glioma cells and active surface for macrophages describes the community of macrophages present in the modeling domain. It is assumed that these two communities have size of 25 µm as length of active surfaces and are in the distance of 5 µm from each other.

Figure 2: Concentrations of CSF-1$_d$ within the domain after 24 hours of macrophage-glioma cell interaction. *The schematic images symbolize the WHO grades of the glioma including 2D-color table, which represents the concentration gradient of CSF-1d, and one-dimensional plot presents the change in the concentration of CSF-1$_d$ in x-direction of the domain.* ***a)*** *The grade I glioma with 2x107 macrophages and 16x10^6 gliomas,* ***b)*** *the grade II glioma with 1x10^7 macrophages and 56x10^6 glioma cells,* ***c)*** *the grade III glioma with 2x10^6 macrophages and 16x10^7 glioma cells, and* ***d)*** *the grade IV glioma with 1x10^6 macrophages and 26x10^7 glioma cells. For all grades of glioma, the initial concentration value of CSF-1$_d$ was set to zero. The simulation time was 24 hours. All color tables are assigned to have minimum (blue) and maximum (red) reference values of 1.76x10^{-26} and 3.45x10^{-16}, respectively. Glioma cells and macrophages are located on their specific active surfaces and the number of cells in each image illustrates in a symbolic way the difference between the number of glioma cells and macrophages. The x-axis stands for the distance between macrophages and glioma cells; the origin is located at the active surface of glioma cells.*

Figure 3: Concentrations of EGF$_d$ within the domain after 24 hours of macrophage-glioma cell interaction. *The schematic images symbolize the WHO grades of the glioma including 2D-color table, which represents the concentration gradient of EGF$_d$, and one-dimensional plot presents the change in the concentration of EGF$_d$ in x-direction of the domain.* ***a)*** *The grade I glioma with 2x10^7 macrophages and 16x10^6 gliomas,* ***b)*** *the grade II glioma with 1x10^7 macrophages and 56x10^6 glioma cells,* ***c)*** *the grade III glioma with 2x10^6 macrophages and 16x10^7 glioma cells, and* ***d)*** *the grade IV glioma with 1x10^6 macrophages and 26x10^7 glioma cells. For all grades of glioma, the initial concentration value of EGF$_d$ was set to zero. The simulation time was 24 hours. All color tables are assigned to have minimum (blue) and maximum*

(red) reference values of 4.25×10^{-30} and 2.67×10^{-17}, respectively. Glioma cells and macrophages are located on their specific active surfaces and the number of cells in each image illustrates in a symbolic way the difference between the number of glioma cells and macrophages. The x-axis stands for the distance between macrophages and glioma cells; the origin is located at the active surface of glioma cells.

Figure 4: Time-dependent concentration changes for CSF-1$_s$ and CSF-1$_d$ for low-grade to high-grade gliomas. a) Concentration of CSF-1$_s$ with respect to time from low-grade glioma to high-grade glioma. **b)** Concentration of CSF-1$_d$ with respect to time from low-grade glioma to high-grade glioma. The initial values of CSF-1$_s$ and CSF-1$_d$ concentration were zero and the simulations were performed for 24 hours. The grade I glioma has 2×10^7 macrophages and 16×10^6 gliomas, the grade II glioma has 1×10^7 macrophages and 56×10^6 glioma cells, the grade III glioma has 2×10^6 macrophages and 16×10^7 glioma cells, and the grade IV glioma has 1×10^6 macrophages and 26×10^7 glioma cells.

Figure 5: Time-dependent concentration changes for EGF$_s$ and EGF$_d$ for low-grade to high-grade gliomas. a) Concentration of EGF$_s$ with respect to time from low-grade glioma to high-grade glioma. **b)** Concentration of EGF$_d$ with respect to time from low-grade glioma to high-grade glioma. The initial values of EGF$_s$ and EGF$_d$ concentration were zero and the simulations were performed for 24 hours. The grade I glioma has 2×10^7 macrophages and 16×10^6 gliomas, the grade II glioma has 1×10^7 macrophages and 56×10^6 glioma cells, the grade III glioma has 2×10^6 macrophages and 16×10^7 glioma cells, and the grade IV glioma has 1×10^6 macrophages and 26×10^7 glioma cells.

Table 1: Table of parameters, their values and references used in simulation.

Table 2: The number of cells and the values of K On-E used in simulations were used from Lu and his co-workers study[47].